

Constraints on neutrino mass from Cosmic Microwave Background and Large Scale Structure

Z. Pan,^{1*} L. Knox^{1†}

¹*Department of Physics, University of California, One Shields Avenue, Davis, CA, USA 95616*

26 November 2021

ABSTRACT

Our tightest upper limit on the sum of neutrino mass eigenvalues M_ν comes from cosmological observations that will improve substantially in the near future, enabling a detection. The combination of the Baryon Acoustic Oscillation feature measured from the Dark Energy Spectroscopic Instrument and a Stage-IV Cosmic Microwave Background experiment has been forecasted to achieve $\sigma(M_\nu) < 1/3$ of the lower limit on M_ν from atmospheric and solar neutrino oscillations (Abazajian et al. 2013; Fogli et al. 2012). Here we examine in detail the physical effects of neutrino mass on cosmological observables that make these constraints possible. We also consider how these constraints would be improved to ensure at least a 5σ detection.

Key words: cosmology – cosmology:cosmic microwave background – cosmology: observations – large-scale structure of universe

1 INTRODUCTION

Basic questions about the neutrino mass matrix remain unanswered, such as whether the CP-violating phase is non-zero, whether the neutrinos are Majorana or Dirac, and whether the hierarchy of masses is normal or inverted (Fogli et al. 2012; Forero, Tórtola & Valle 2012; Barger, Marfatia & Whisnant 2002). Significant experimental and observational efforts are underway and being planned to answer these questions. Doing so may shed light on possible extensions beyond the standard model of particle physics.

The question of the type of mass hierarchy may be settled by cosmological observations. The best lower limit on the sum of the mass eigenstate masses, M_ν , comes from analysis of solar and atmospheric neutrino oscillation data (Forero, Tórtola & Valle 2014). If cosmological determinations of this quantity tighten up near this lower bound, then the inverted hierarchy will be ruled out.

Current data lead to $0.058 \text{ eV} \lesssim M_\nu \lesssim 0.21 \text{ eV}$, where the upper limit comes from cosmic microwave background (CMB) and baryon acoustic oscillation (BAO) data (Planck Collaboration XIII 2015). Bringing this upper limit down is a major science goal of a Stage-IV (S4) cosmic microwave background project, CMB-S4, and also of the galaxy survey project Dark Energy Spectroscopic Instrument (DESI). These projects are forecasted to determine M_ν with a one-standard deviation of 45 meV (CMB-S4 alone) and 16 meV (CMB-S4 combined with DESI BAO) (Abazajian et al.

2013). These uncertainties are small enough to guarantee a detection of $M_\nu \neq 0$ at a 3σ or greater confidence level.

Of course any conclusions from such cosmological data will be model dependent. How convincing will these data be that we are indeed seeing the impact of neutrino mass, and not misinterpreting some other signals? The forecasted precision is also not quite as strong as one would like; is there a way to guarantee at least a 5σ detection of $M_\nu \neq 0$? Here we address these questions. To address the first question we examine the particular signatures of neutrino mass that lead to the above forecasts. To address the second we look at what additional types of data can further tighten the expected uncertainties.

The paper is organized as follows. In Section 2, we briefly introduce the cosmological signatures of massive neutrinos. In Section 3, we focus on changes in the cosmic expansion rate and structure growth rate due to massive neutrinos. In Section 4, we analyze the influence of massive neutrinos on the CMB lensing potential power spectrum. Forecasts on the constraints of total neutrino mass from CMB and Large Scale Structure (LSS) measurements are given in Section 5 and conclusions are presented in Section 6.

2 SIGNATURES OF NON-ZERO NEUTRINO MASS

The cosmological signatures of massive neutrino have been investigated since decades ago, e.g. (Doroshkevich et al. 1980; Doroshkevich & Khlopov 1981; Doroshkevich et al. 1981). We can more broadly view the cosmological neutrino

* Email: zhpan@ucdavis.edu

† Email: lknox@ucdavis.edu

program as a study of the dark radiation that we know exists as a thermal relic of the big bang. By dark radiation here we mean anything, other than photons, thermally produced in the early universe that is relativistic at least through decoupling. We know that such a background of nearly massless non-photon radiation exists with high confidence from light element abundances and the cosmic microwave background damping tail. Both are sensitive to the history of the expansion rate, which depends on the mean density via the Friedmann equation. Combining Helium abundance and CMB data constrains the effective number of relativistic species to be $N_{\text{eff}} = 2.99 \pm 0.39$ (Planck Collaboration XIII 2015).

Is this background entirely that of the 3 active neutrino species? Is any part of it from something else? Could there be a significant excess of neutrinos over anti-neutrinos? These are interesting questions, also to be addressed by future CMB observations that will significantly tighten up constraints on N_{eff} . Our confidence that the dark radiation is indeed that of cosmological neutrinos with phase-space distributions as expected from the standard thermal history will be greatly increased if the constraints on N_{eff} tighten up to $\sigma(N_{\text{eff}}) = 0.02$, as forecasted, consistent with the expected value of 3.046. For the purposes of this paper, we will assume this is what will happen.

If we assume that the dark radiation background is entirely the active neutrinos with the expected phase space distributions, the assumption of non-zero neutrino mass leads to very specific predictions for cosmological observables. First we consider the expansion rate as a function of redshift. The rest-mass energy of the neutrinos begins to slow down the decline of energy density with expansion as they become non-relativistic, leading to an increase in $H(z)$ relative to the $M_\nu = 0$ expectation. This increase would persist to $z = 0$ if we were holding the other contents of the low-redshift universe constant. However, for our purposes of exploring observable consequences of $M_\nu \neq 0$ it makes much more sense to hold the angular size of the sound horizon on the last-scattering surface constant, since this quantity is so well-determined from CMB observations (Planck Collaboration XIII 2015; Hinshaw et al. 2013). To do so one must decrease the density of dark energy. Assuming the dark energy is a cosmological constant, the shape of $\Delta H(z)$ has a very particular form, as shown in Fig. 1, changing sign very near $z = 1$, with the onset of dark energy domination.

Were we able to trace out this departure of $H(z)$ from the $M_\nu = 0$ shape, it would contribute to our confidence we are seeing the impact of non-zero neutrino mass. However, as we will see, the DESI determinations of $H(z)$ will be insufficient to resolve this very small signal across redshift. That is not to say the signal is altogether observably invisible. These changes to $H(z)$ affect comoving angular diameter distance $D_A(z)$ in ways that are detectable by DESI. It is just that it will be difficult, if not impossible, to make the case that there is the sign change in the $H(z)$ correction near $z \simeq 1$. The changes to $H(z)$ also directly impact the growth of structure, with observable consequences for the redshift-space distortion (RSD) and the CMB lensing potential power spectrum, which we will discuss in Section 3 and 4 respectively.

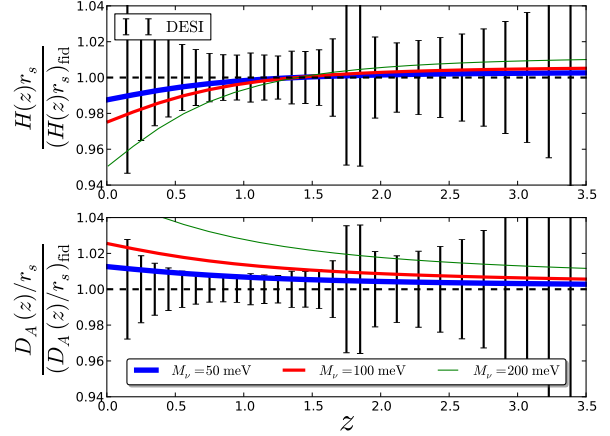


Figure 1. The dependence of expansion rate $H(z)$ and comoving angular diameter distance $D_A(z)$ on M_ν , where we minimize the $\chi^2(\Theta, M_\nu)$ by adjust the 6 Λ CDM parameters Θ when increasing M_ν from 0 to 50, 100, 200 meV.

3 INFLUENCE OF MASSIVE NEUTRINOS ON GALAXY SURVEY OBSERVABLES

To quantify the influence of massive neutrinos, we compare a fiducial cosmology with massless neutrinos and a cosmology with massive neutrinos. The fiducial cosmology is a flat Λ CDM universe with the *Planck* best fit parameters (Planck Collaboration XVI 2014), i.e. $\omega_b = 0.022032$, $\omega_m = 0.14305$, $A_s = 2.215 \times 10^{-9}$, $n_s = 0.9619$, $\tau = 0.0925$, $H_0 = 67.04$ km/s/Mpc, $M_\nu = 0$ meV. The set of $M_\nu \neq 0$ cosmologies have parameters $\theta = (\Theta, M_\nu)$, where Θ are Λ CDM parameters. Given a specific M_ν , we choose Θ by minimizing $\chi^2(\Theta, M_\nu)$, with

$$\begin{aligned} \chi^2(\Theta, M_\nu) &= F_{\alpha\beta} \lambda_\alpha \lambda_\beta \\ &= F_{ij} \lambda_i \lambda_j + 2F_{i\nu} \lambda_i M_\nu + F_{\nu\nu} M_\nu^2, \end{aligned} \quad (1)$$

where F is the Fisher matrix for the CMB observations, $\lambda_i = (\Theta - \Theta_{\text{fid}})_i$ with i indexing the 6 Λ CDM parameters and summation over repeated indexes α, β, i, j is implied. Minimizing $\chi^2(\Theta, M_\nu)$ requires

$$0 = \partial\chi^2/\partial\lambda_i \rightarrow \lambda_i = -(G^{-1})_{ij} F_{j\nu} M_\nu, \quad (2)$$

where G is a subset of the Fisher matrix F , $G_{ij} \equiv F_{ij}$.

In Fig. 1, we show the influence of $M_\nu = 50, 100$ and 200 meV on expansion rate $H(z)$ and comoving angular diameter distance $D_A(z)$. We see that $H(z \lesssim 1)$ decreases and $H(z \gtrsim 1)$ increases compared to the fiducial cosmology, and the comoving distance $D_A(z)$ increases accordingly. Though the departure of $H(z)$ from the $M_\nu = 0$ shape is undetectable by DESI BAO, the changes in $D_A(z)$ are readily detectable (Font-Ribera et al. 2014).

One of the observable consequences of these changes to $H(z)$ is the impact on the structure growth rate. How one describes this impact depends on what one is using for a comparison model. We use, as a comparison model, a cosmology with massless neutrinos in place of the massive ones. One could also use as a comparison model one with additional cold dark matter in place of the neutrinos. We use the former, consistent with our underlying assumption that

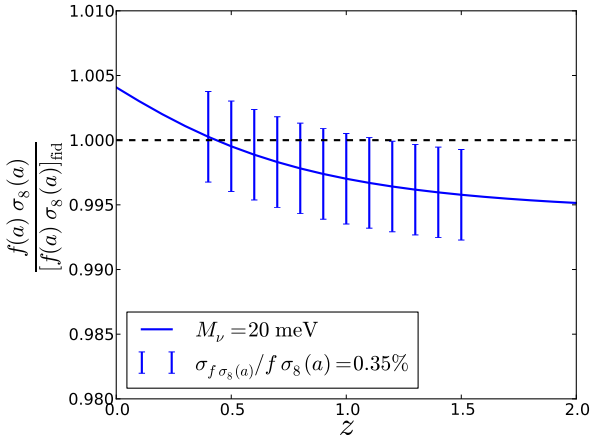


Figure 2. The dependence of structure growth rate on M_ν , where we minimize the $\chi^2(\Theta, M_\nu)$ by adjust the 6 Λ CDM parameters Θ when increasing M_ν from 0 to 20 meV.

we have 3 neutrino species with phase-space distributions as expected from the standard thermal history.

The structure growth rate that is usually quantified by $d \ln \sigma_8(a) / d \ln a$, can be determined by RSD from galaxy surveys, where $\sigma_8(a)$ is the amplitude of mass fluctuations σ_R on scale of $8h^{-1}$ Mpc, i.e., $\sigma_8(a) \equiv \sigma(R = 8h^{-1} \text{Mpc}; a)$. Here

$$\sigma_R^2(a) \equiv \int_0^\infty \frac{k^3}{2\pi^2} P_\delta(k; a) W^2(kR) d \ln k, \quad (3)$$

where $P_\delta(k, a)$ is the matter power spectrum defined by, $\langle \delta(\mathbf{k}; a) \delta^*(\mathbf{k}'; a) \rangle = P_\delta(k; a) \delta^{(3)}(\mathbf{k} - \mathbf{k}')$, and $W(kR) = 3j_1(kR)/kR$ is the window function. Introducing the growth function $D(a)$,

$$D(a) \equiv \frac{\delta(a)}{\delta(a=1)} = \frac{\sigma_8(a)}{\sigma_8(a=1)}, \quad (4)$$

where $\delta(a)$ is the matter overdensity at redshift $z = 1/a - 1$, and defining perturbation growth rate $f(a) \equiv d \ln D(a) / d \ln a$ (Pierpaoli, Scott & White 2001), we may rewrite the structure growth rate as $d \ln \sigma_8(a) / d \ln a = f(a) \sigma_8(a)$.

In the above definition, the growth function $D(a)$ and the structure growth rate $f(a) \sigma_8(a)$ depend on $\sigma_8(a=1)$ which varies for our fiducial $M_\nu = 0$ model and the model with massive neutrinos. For easier comparison, we introduce the growth function $D_e(a)$ normalized at early time, say at $a_e = 1/1100$ when massive neutrinos are relativistic,

$$D_e(a) \equiv \frac{\delta(a)}{\delta(a_e)} = \frac{\sigma_8(a)}{\sigma_8(a_e)}, \quad (5)$$

and the structure growth rate can be rewritten as

$$f(a) \sigma_8(a) = \frac{dD_e(a)}{d \ln a} \sigma_8(a_e), \quad (6)$$

where $\sigma_8(a_e)$ is the same for the model with massive neutrinos and the fiducial model. So the variation of $f(a) \sigma_8(a)$ only depends on the growth rate $dD_e(a)/da$.

In Fig. 2, we show the impact of massive neutrinos with mass 20 meV on the structure growth rate. The structure growth rate is decreased at high redshift because of the enhanced expansion rate (Fig. 1). Note though that the tran-

sition of structure growth rate from suppressed to enhanced is delayed to $z \simeq 0.5$ compared to $z \simeq 1$ when the expansion rate transitions. The reason for this delay is that the growth rate $dD_e(a)/da$ is determined by two factors: the expansion rate and gravitational attraction. The slower growth at $z \lesssim 1$ leads to weaker gravitational potentials. Around $z \simeq 1$, the expansion rate is the same for the two models, but the gravitational potential is weaker for the $M_\nu \neq 0$ model. Therefore the growth rate remains suppressed, until some later time $z \simeq 0.5$ when the weaker gravitational potential is compensated by even slower expansion.

DESI will provide a comprehensive survey of spectroscopic galaxies and quasars covering redshifts $0.1 < z < 3.5$, with precision in each redshift bin $\Delta z = 0.1$ better than $\sigma_{f\sigma_8(a)}/f\sigma_8(a) = 0.35\%$ from $0.4 < z < 1.5$ (Huterer et al. 2013). In Fig. 2, we show the influence of $M_\nu = 20$ meV on the structure growth rate $f(a) \sigma_8(a)$, which is detectable by DESI RSD.

4 INFLUENCE OF MASSIVE NEUTRINOS ON THE CMB LENSING POWER SPECTRUM

4.1 Introduction to the lensing power spectrum

We begin with a brief review of gravitational lensing of the CMB. For details see e.g. the review by Lewis & Challinor (2006). Gradients in the gravitational potential, Φ , distort the trajectories of photons traveling to us from the last scattering surface. The deflection angles, in Born approximation, are $\mathbf{d} = \nabla \phi$, where the lensing potential, ϕ , is a weighted radial projection of Φ . The key quantity for calculating the impact of lensing on the temperature power spectrum is the angular power spectrum of the projected potential, $C_\ell^{\phi\phi}$, which we also call the lensing power spectrum. Taking advantage of the Limber approximation (Limber 1953), it can be written as a radial integral over the three dimensional gravitational potential power spectrum P_Φ

$$\ell^4 C_\ell^{\phi\phi} \simeq 4 \int_0^{\chi_*} d\chi (k^4 P_\Phi) \left(\frac{\ell}{\chi}; a \right) \left[1 - \frac{\chi}{\chi_*} \right]^2, \quad (7)$$

where χ is the comoving distance from the observer, $a = a(\chi)$, a \star subscript indicates the last scattering surface, $(1 - \chi/\chi_*)^2$ is the lensing kernel, and the power spectrum P_Φ is defined as

$$\langle \Phi(\mathbf{k}; a) \Phi^*(\mathbf{k}'; a) \rangle = P_\Phi(k; a) \delta^{(3)}(\mathbf{k} - \mathbf{k}'). \quad (8)$$

To calculate P_Φ we assume a power-law primordial power spectrum $P_\Phi^p(k)$,

$$\frac{k^3}{2\pi^2} P_\Phi^p(k) = A_s \left(\frac{k}{k_0} \right)^{n_s - 1}, \quad (9)$$

where k_0 is an arbitrary pivot point, A_s and n_s are the primordial amplitude and power law index respectively.

The gravitational potential at late times, $\Phi(k, a)$, is related to the primordial potential $\Phi^p(k)$ by (e.g. Kodama & Sasaki 1984)

$$\Phi(k, a) = \frac{9}{10} \Phi^p(k) T(k) s(k; a) g(a), \quad (10)$$

where the potential on very large scales is suppressed by a

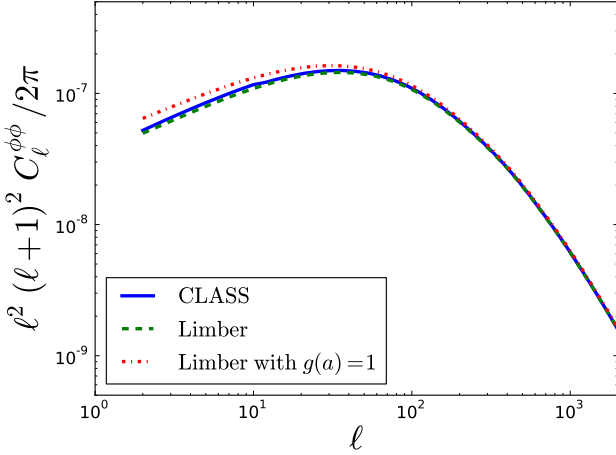


Figure 3. The lensing power spectrum calculated from CLASS (solid line), calculated with Limber approximation (dashed line) and calculated with Limber approximation and setting $g(a) = 1$ (dashed-dotted line).

factor 9/10 through the transition from radiation domination to matter domination. For modes which enter the horizon during radiation domination when the dominant component has significant pressure ($p \approx \rho/3$) the amplitude of perturbations cannot grow and the expansion of the Universe forces the potentials to decay. In a cosmology with massless neutrinos, for modes which enter the horizon after matter-radiation equality (but before dark energy domination) the potentials remain constant. The transfer function $T(k)$ takes this into account, being unity for very large scale modes and falling approximately as k^{-2} for small scales. The transfer function $T(k)$ is independent of scale factor a because in a cosmology with massless neutrinos, potentials on all scales keep constant in matter domination. The impact of massive neutrinos on the potentials is described by the function, $s(k; a)$, which is unity on scales above the free-streaming scale and decreases with time on scales below. Once the cosmological constant starts to become important the potentials on all scales begin to decay. This effect is captured by the growth function, $g(a)$, which is unity during matter domination. With these definitions we have

$$(k^4 P_\Phi)(k; a) = \frac{81}{50} \pi^2 g^2(a) s^2(k; a) k T^2(k) A_s \left(\frac{k}{k_0} \right)^{n_s - 1}. \quad (11)$$

With these pieces in place, we now examine the accuracy of the Limber approximation. According to [Loverde & Afshordi \(2008\)](#), it is a better approximation to replace $k = \ell/\chi$ with $\sqrt{\ell(\ell+1)}/\chi \simeq (\ell+0.5)/\chi$ in the original Limber approximation Eq.(7). With the replacement and defining $x = \chi/\chi_*$, the lensing power spectrum can be written as

$$\ell^2 (\ell + 1)^2 C_\ell^{\phi\phi} \simeq 4\chi_* \int_0^1 dx (k^4 P_\Phi) \left(\frac{\ell + 0.5}{x\chi_*}; a \right) (1-x)^2, \quad (12)$$

where $a = a(x)$. Fig. 3 shows the lensing power spectrum calculated from CLASS ([Lesgourgues 2011a,b](#); [Blas, Lesgourgues & Tram 2011](#); [Lesgourgues & Tram 2011](#)) compared to the lensing power spectrum calculated from the Limber approximation. We see the Limber approximation reproduces

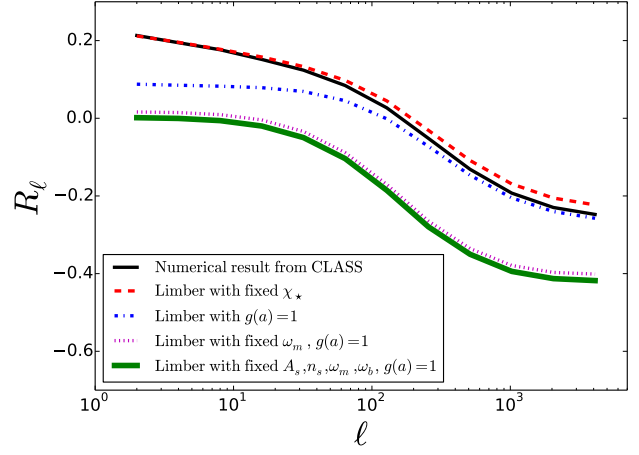


Figure 4. The dependence of the lensing power spectrum on total neutrino mass, $(C_\ell^{\phi\phi} - C_{\ell, \text{fid}}^{\phi\phi})/C_{\ell, \text{fid}}^{\phi\phi} = R_\ell \times (M_\nu/\text{eV})$. The black line is the numerical result from CLASS, the red line is the result of Limber approximation setting $\chi_* = 1.4 \times 10^4$ Mpc, the blue line is the result of Limber approximation with $g(a) = 1$, the magenta line is the result of Limber approximation fixing both ω_m and $g(a)$, and green line is the result of Limber approximation with $A_s, n_s, \omega_m, \omega_b$ and $g(a)$ fixed.

the accurate numerical result even for small ℓ . In order to understand the the influence of the growth function, we also calculated the lensing power spectrum by setting $g(a) \equiv 1$. The growth function makes a difference for $\ell \lesssim 50$ ([Pan, Knox & White 2014](#)). Now we are to understand the impact of massive neutrinos on $C_\ell^{\phi\phi}$.

4.2 Influence of massive neutrinos on the lensing power spectrum: results

According to Eq.(11) and Eq.(12), it is clear that $C_\ell^{\phi\phi}$ is determined by the primordial perturbation A_s, n_s , the transfer function $T(k)$, the impact of massive neutrinos $s(k; a)$, the growth factor $g(a)$, and the comoving distance to the last scattering surface χ_* .

In order to quantify the dependence of the lensing power on total neutrino mass M_ν , we take samples from a *Planck* $\Lambda\text{CDM} + M_\nu$ chain, and fit the linear relation

$$\frac{C_\ell^{\phi\phi} - C_{\ell, \text{fid}}^{\phi\phi}}{C_{\ell, \text{fid}}^{\phi\phi}} = R_\ell \times M_\nu (\text{eV}), \quad (13)$$

The linear fitting result is shown as the thin solid line in Fig. 4. To understand the contribution of the various parameter variations and effects, we also plot R_ℓ in Fig. 4 for the cases shown.

We now work our way towards an understanding of the full response, the thin solid curve, in stages. We begin with the case where we fix most of the parameters other than M_ν , and turn off the impact of dark energy on the growth factor, $g(a)$, fixing it to unity. In this case, increasing M_ν has two effects: 1) it decreases the free-streaming length $\sim (T_\nu/M_\nu)/H(z)$ ([Abazajian et al. 2011](#)), and 2) increases the expansion rate once the neutrinos start to become non-relativistic. The increased expansion rate acts to suppress the growth of structure on all length scales. However, the de-

creased free-streaming length acts to boost structure growth on scales above the free-streaming length, nearly exactly canceling the suppression. The result is the bottom-most curve of Fig. 4: nearly no effect at low ℓ , a constant suppression of power at high ℓ , and a smooth transition between these two regimes.

The difference between the bottom-most curve and the dot-dashed curve (the one labeled, ‘Limber with $g(a) = 1$ ’) is due to how other parameters adjust as M_ν varies. We can isolate these changes as almost all due (at least at $\ell \gtrsim 50$) to a correlation between M_ν and ω_m , as demonstrated by the following: if we fix ω_m , and let A_s , n_s , and ω_b vary, we get the second curve from the bottom which differs very little from the bottom-most curve. Once we let ω_m vary as well, we get the dot-dashed curve. Letting ω_m vary leads to variation in n_s and A_s as well, but these changes all flow from the correlation between ω_m and M_ν .

Once we let $g(a)$ vary as well we get a curve that is indistinguishable from the thin solid curve, which is boosted everywhere, and especially at $\ell \lesssim 50$. The contributions to these large angular scales come predominantly from modes to the left of the peak in the matter power spectrum. At fixed (large) angular scale, structures that are nearer by, and therefore on smaller length scales, are closer to the peak of the matter power spectrum. Thus the large angular scales are weighted toward later times, and therefore more influenced by $g(a)$ than the smaller angular scales. The growth factor *increases* with increasing M_ν because to keep the angular size of the sound horizon fixed Ω_Λ must decrease.

The lensing kernel’s dependence on cosmological parameters comes entirely via its dependence on χ_* . To see how much of the variation in the lensing power spectrum is due to the lensing kernel, we fix $\chi_* = 1.4 \times 10^4$ Mpc (top-most dashed curve). By examining the difference between the top-most dashed curve, for which χ_* is fixed, and the thin solid curve, which is the full numerical result, one can see this effect is very small¹

¹ This result is in contrast to the case of tomographic cosmic shear as a probe of dark energy. In this case the sensitivity of the data to variations in the dark energy equation-of-state parameter largely arises from the lensing kernel (Simpson & Bridle 2005; Zhang, Hui & Stebbins 2005).

To summarize, there are three main effects of massive neutrinos on the lensing power: 1) increased expansion rate suppresses power, 2) decreased free-streaming length compensates for the suppressed power at scales above the free-streaming length, 3) other parameter variations due to partial degeneracies in C_l^{TT} (most notably an increase in ω_m) boost the power on all scales. The net result is increased power at large scales and a decrease in power at small scales. One might potentially include the growth factor here as the fourth-most important effect, somewhat increasing the power at large angular scales.

The origin of the degeneracy in C_l^{TT} between ω_m and M_ν is actually due to lensing itself. Planck Collaboration XVI (2014) demonstrated that the dominant effect leading to the constraint of neutrino mass from the CMB temperature anisotropy power spectrum is gravitational lensing. As shown in Fig. 4, increasing M_ν suppresses the lensing power, while increasing ω_m increases the lensing power. The lensing power suppression by massive neutrinos can be compensated by the enhancement from increasing ω_m , so uncertainties in M_ν and ω_m are expected to be positively correlated (Namikawa, Saito & Taruya 2010).

5 FORECAST OF CONSTRAINTS ON THE TOTAL NEUTRINO MASS FROM DIFFERENT DATA SETS

We use the Fisher matrix formalism to forecast constraints on neutrino mass from future CMB and LSS experiments. The fiducial cosmology used here is the same as the one used in Section 3 except with a different value of total neutrino mass, $M_\nu = 85$ meV.

5.1 CMB-S4 and DESI BAO

Following Wu et al. (2014) and Dodelson (2003), the Fisher matrix for cosmological parameters constrained by CMB spectra is written as

$$F_{\alpha\beta} = \sum_{\ell}^{\ell_{\max}} \frac{2\ell + 1}{2} f_{\text{sky}} \text{Tr} \left(C_{\ell}^{-1} \frac{\partial C_{\ell}}{\partial \theta_{\alpha}} C_{\ell}^{-1} \frac{\partial C_{\ell}}{\partial \theta_{\beta}} \right), \quad (14)$$

and it is related to the expected uncertainty of a parameter θ_{α} by $\sigma(\theta_{\alpha}) = \sqrt{(F^{-1})_{\alpha\alpha}}$, where

$$C_{\ell} = \begin{pmatrix} C_{\ell}^{TT} + N_{\ell}^{TT} & C_{\ell}^{TE} & C_{\ell}^{Td} \\ C_{\ell}^{TE} & C_{\ell}^{EE} + N_{\ell}^{EE} & 0 \\ C_{\ell}^{Td} & 0 & C_{\ell}^{dd} + N_{\ell}^{dd} \end{pmatrix}, \quad (15)$$

and C_{ℓ}^{dd} is the angular power spectrum of the deflection field \mathbf{d} , which is related to the lensing power spectrum by $C_{\ell}^{dd} = \ell(\ell + 1)C_{\ell}^{\phi\phi}$. The Gaussian noise N_{ℓ}^{XX} is defined as

$$N_{\ell}^{XX} = \Delta_X^2 \exp \left(\ell(\ell + 1) \frac{\theta_{\text{FWHM}}^2}{8 \log 2} \right), \quad (16)$$

where Δ_X ($X = T, E, B$) is the pixel noise level of the experiment and θ_{FWHM} is the full-width-half-maximum beam size in radians (Knox 1995; Zaldarriaga, Spergel & Seljak 1997). The noise power spectrum of deflection field N_{ℓ}^{dd} is calculated assuming a lensing reconstruction that uses the quadratic EB estimator (Okamoto & Hu 2003). We use the iterative method proposed by Smith et al. (2012), which performs significantly better than the uniterated quadratic estimators (Hirata & Seljak 2003).

For the CMB-S4 experiment, we assume the temperature noise level $\Delta_T = 1.5 \mu\text{K-arcmin}$, the polarization noise level $\Delta_E = \Delta_B = \sqrt{2} \Delta_T$, the fraction of covered sky $f_{\text{sky}} = 0.5$ and the beam size $\theta_{\text{FWHM}} = 1'$. With these given experiment sensitivities, we obtain a constraint from CMB with $\sigma(M_\nu) = 38$ meV. The 1σ and 2σ constraint are shown in Fig. 5.

According to the analysis in Section 3 and 4, DESI BAO are helpful to break the degeneracy between M_ν and ω_m . BAO uncertainties are independent from CMB experiments, so the total Fisher matrix is simply given by addition

$$F_{\text{CMB+BAO}} = F_{\text{CMB}} + F_{\text{BAO}}, \quad (17)$$

where the DESI sensitivities of BAO signal can be found in Font-Ribera et al. (2014) and shown in Fig. 1. It is found that, adding the DESI BAO data greatly improves the constraint to $\sigma(M_\nu) = 15$ meV (similar forecasts were also conducted by Abazajian et al. (2013); Wu et al. (2014)).

5.2 Beyond DESI BAO

The largest signal of massive neutrinos on $H(z)$ and $D(z)$ is found at low redshifts (see Fig. 1), where BAO has inevitably

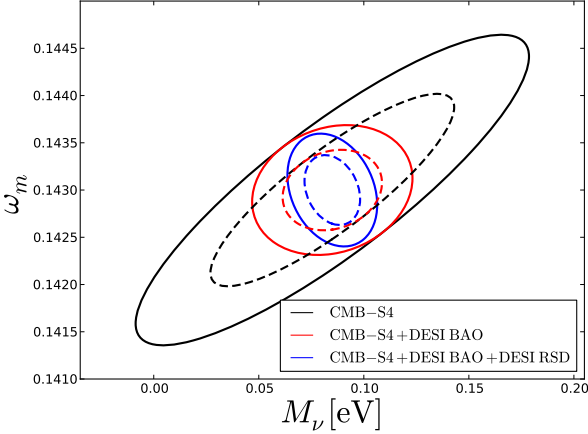


Figure 5. Forecasted 1σ and 2σ constraints in the $M_\nu - \omega_m$ plane, where the CMB-S4 experiment results in a $\sigma(M_\nu) = 38$ meV constraint, the combination of CMB-S4 and DESI BAO yield a $\sigma(M_\nu) = 15$ meV constraint, and adding measurements of the structure growth rate by DESI RSD further improves the constraint to $\sigma(M_\nu) = 9$ meV.

large noise because of small amount of survey volume and large cosmic variance. Other than DESI BAO, we also investigate other low-redshift tracers of $H(z)$ and $D(z)$ which are possible to tighten the uncertainty of total neutrino mass.

DESI RSD: similar to BAO, RSD uncertainties are also independent from those of CMB observations, so the total Fisher matrix of CMB+BAO+RSD is also approximately given by addition

$$F_{\text{CMB+BAO+RSD}} = F_{\text{CMB}} + F_{\text{BAO}} + F_{\text{RSD}}, \quad (18)$$

where we use the RSD sensitivities from DESI survey which can be found in [Huterer et al. \(2013\)](#) and shown in Fig. 2. Here we use the approximation that uncertainties in BAO and RSD are uncorrelated, due to they are sensitive to different aspects of the matter power spectrum: BAO is sensitive to its characteristic length scale r_s while RSD is sensitive to its amplitude. In fact, our result is insensitive to the approximation because we find that both CMB-S4+DESI BAO+DESI RSD and CMB-S4+DESI RSD yield the same $\sigma(M_\nu) = 9$ meV uncertainty.

Better BAO: DESI survey cover 14,000 squared degrees (about 1/3 of the whole sky). We explore a future BAO experiment which covers the whole sky and in which cosmic variance dominates over shot noise in the redshift range $0 < z < 4.0$. Constraints on $D_A(z)$ and $H(z)$ from this BAO experiment are shown in Fig. 6. It is found that CMB-S4 and the cosmic variance limited BAO constrain the total neutrino mass with uncertainty $\sigma(M_\nu) = 11$ meV. So we conclude that 11 meV is a lower limit of $\sigma(M_\nu)$ we could measure from CMB-S4+BAO, where the limit mainly comes from noise level of the CMB lensing signal.

Supernovae: The constraining power of BAO is limited by its large cosmic variance at low redshifts (Fig. 6), so supernovae distance measurements which do not suffer from the cosmic variance problem may be effective complements if their systematic errors are well controlled. Supernovae perform better in relative distance measurements than in absolute distance measurements. However for the $\Lambda\text{CDM} + M_\nu$

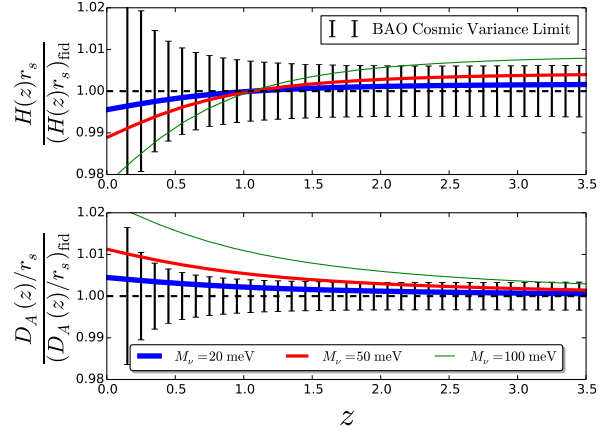


Figure 6. Same as Fig. 1, but with suppressed errorbars of $D_A(z)$ and $H(z)$ coming from CMB-S4 and a cosmic-variance-limited BAO experiment.

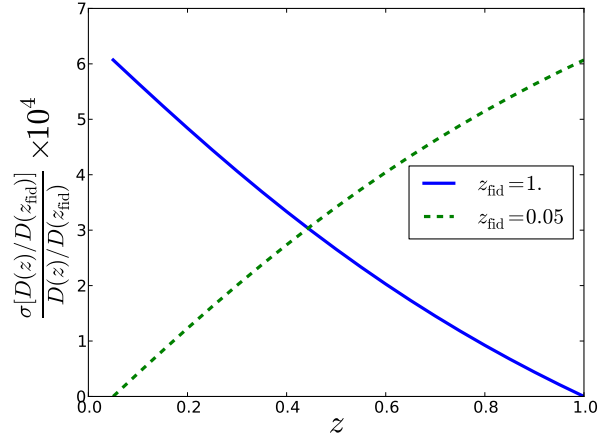


Figure 7. The uncertainties in relative distances from CMB-S4 + DESI BAO. Note that the uncertainties is multiplied by a factor of 10^4 in the plot.

model, the uncertainties in relative distances from CMB-S4 + DESI BAO are very small (see Fig. 7). We conclude that supernova observations must result in relative distance determinations with systematic errors less than about 0.05% if they are to tighten the constraints on neutrino mass. Compared to systematic errors from current supernova observations (e.g., [Suzuki et al. \(2012\)](#)) this would be a reduction by a factor of ~ 20 .

6 CONCLUSION

This paper is motivated by our desire to better understand the origin of current and forecasted cosmological constraints on the sum of neutrino masses. We took as a given that determination of N_{eff} will solidify the predicted value of 3.046, increasing our confidence that the phase-space distribution of the cosmic neutrino background is what we expect based on the standard thermal history. With that as a given, the most important aspect of increased neutrino mass (relative

to some reference model) is an increased neutrino energy density. If the model with increased mass is to remain consistent with CMB observations, the distance to last-scattering must be preserved and so the total energy density, and therefore the expansion rate, cannot increase at all redshifts. To compensate for the increase in neutrino energy density, the cosmological constant must decrease in value. Thus varying neutrino mass leads to changes in $H(z)$ with a very particular shape: a mild increase at high redshifts, a larger decrease in low redshifts, with a transition near the onset of Λ -domination at $z \simeq 1$. Unfortunately this very specific prediction of the shape for $H(z)$ is difficult to verify in detail because of how small the departures from the reference model are at $z > 1$. We see that this difficulty persists even for a cosmic-variance limited all-sky ($z < 4$) BAO experiment (see Fig. 6).

The sensitivity of CMB-S4 to neutrino mass comes via the impact of this increased expansion rate on the growth of structure. At scales below the neutrino free-streaming length, this increased expansion rate suppresses the growth of structure. Above the free-streaming length, the ability of massive neutrinos to cluster compensates for the increased expansion and there is no net suppression. Because increasing matter density increases lensing power amplitude, the CMB lensing-derived constraints on neutrino mass have uncertainties positively correlated with the matter density uncertainties. This correlation with dark matter density leads to secondary correlations of neutrino mass uncertainty with uncertainties in n_s and A_s . We disentangled all these various effects in Fig. 4.

The correlation between M_ν and ω_m has the opposite sign as that from BAO, since increasing neutrino mass and increasing ω_m both increase the expansion rate at $z > 1$, and lead to a compensating decrease at $z < 1$. Thus the combination of CMB-S4 and DESI-BAO leads to improvements in the determination of both quantities.

Finally, we briefly investigated how constraints might be improved beyond the $\sim 3\sigma$ to $\sim 4\sigma$ detection expected from CMB-S4 + DESI BAO in the case of the lowest possible neutrino mass of 58 meV. The larger signals are at low redshift, so we considered supernovae as relative distance indicators and redshift-space distortions, as well as cosmic-variance-limited BAO. We found requirements on supernova precision that are probably prohibitively stringent. But better BAO, and RSD, both have the potential to improve the detection to $\sim 5\sigma$ or greater.

7 ACKNOWLEDGMENTS

We thank Anze Slosar and Patrick McDonald for sharing the forecasts from DESI BAO. Z.P. would like to thank Brent Follin for introducing CLASS code and Marius Millea for python package `Cosmoslik`. This work made extensive use of the NASA Astrophysics Data System and of the `astro-ph` preprint archive at [arXiv.org](https://arxiv.org).

REFERENCES

Abazajian K. N. et al., 2013, preprint(arXiv:1309.5383)
 Abazajian K. N. et al., 2011, *Astroparticle Physics*, 35, 177

Barger V., Marfatia D., Whisnant K., 2002, *Phys. Rev. D*, 65, 073023
 Blas D., Lesgourgues J., Tram T., 2011, *J. of Cosm. & Astropart. Phys.*, 7, 34
 Dodelson S., 2003, *Modern cosmology*
 Doroshkevich A. G., Khlopov M. I., Sunyaev R. A., Szalay A. S., Zeldovich I. B., 1981, *Annals of the New York Academy of Sciences*, 375, 32
 Doroshkevich A. G., Khlopov M. Y., 1981, *Astronomicheskii Zhurnal*, 58, 913
 Doroshkevich A. G., Zeldovich Y. B., Syunyaev R. A., Khlopov M. Y., 1980, *Pisma v Astronomicheskii Zhurnal*, 6, 457
 Fogli G. L., Lisi E., Marrone A., Montanino D., Palazzo A., Rotunno A. M., 2012, *Phys. Rev. D*, 86, 013012
 Font-Ribera A., McDonald P., Mostek N., Reid B. A., Seo H.-J., Slosar A., 2014, *J. of Cosm. & Astropart. Phys.*, 5, 23
 Forero D. V., Tórtola M., Valle J. W. F., 2012, *Phys. Rev. D*, 86, 073012
 Forero D. V., Tórtola M., Valle J. W. F., 2014, *Phys. Rev. D*, 90, 093006
 Hinshaw G. et al., 2013, *ApJS*, 208, 19
 Hirata C. M., Seljak U., 2003, *Phys. Rev. D*, 68, 083002
 Huterer D. et al., 2013, preprint(arXiv:1309.5385)
 Knox L., 1995, *Phys. Rev. D*, 52, 4307
 Kodama H., Sasaki M., 1984, *Progress of Theoretical Physics Supplement*, 78, 1
 Lesgourgues J., 2011a, ArXiv e-prints
 Lesgourgues J., 2011b, ArXiv e-prints
 Lesgourgues J., Tram T., 2011, *J. of Cosm. & Astropart. Phys.*, 9, 32
 Lewis A., Challinor A., 2006, *Phys. Rep*, 429, 1
 Limber D. N., 1953, *ApJ*, 117, 134
 Loverde M., Afshordi N., 2008, *Phys. Rev. D*, 78, 123506
 Namikawa T., Saito S., Taruya A., 2010, *J. of Cosm. & Astropart. Phys.*, 12, 27
 Okamoto T., Hu W., 2003, *Phys. Rev. D*, 67, 083002
 Pan Z., Knox L., White M., 2014, *MNRAS*, 445, 2941
 Pierpaoli E., Scott D., White M., 2001, *MNRAS*, 325, 77
 Planck Collaboration XIII, 2015, preprint(arXiv:1502.01589)
 Planck Collaboration XVI, 2014, *A&A*, 571, A16
 Simpson F., Bridle S., 2005, *Phys. Rev. D*, 71, 083501
 Smith K. M., Hanson D., LoVerde M., Hirata C. M., Zahn O., 2012, *J. of Cosm. & Astropart. Phys.*, 6, 14
 Suzuki N. et al., 2012, *ApJ*, 746, 85
 Wu W. L. K., Errard J., Dvorkin C., Kuo C. L., Lee A. T., McDonald P., Slosar A., Zahn O., 2014, *ApJ*, 788, 138
 Zaldarriaga M., Spergel D. N., Seljak U., 1997, *ApJ*, 488, 1
 Zhang J., Hui L., Stebbins A., 2005, *ApJ*, 635, 806